Surface termination of $CePt_5$/Pt(111): The key to chemical inertness

C. Praetorius,[1] M. Zinner,[1] G. Held,[2] and K. Fauth[1,3,*]

[1]*Physikalisches Institut, Universität Würzburg, Am Hubland, 97074 Würzburg, Germany*

[2]*Department of Chemistry, University of Reading, Whiteknights Reading RG6 5XS, United Kindgom*

[3]*Wilhelm Conrad Röntgen-Center for Complex Material Systems (RCCM), Universität Würzburg, Am Hubland, 97074 Würzburg, Germany*

(Received 20 August 2015; published 23 November 2015)

The surface termination of $CePt_5$/Pt(111) is determined experimentally by LEED-IV. In accordance with recent theoretical predictions, a dense Pt terminated surface is being found. Whereas the $CePt_5$ volume lattice comprises Pt kagome layers, additional Pt atoms occupy the associated hole positions at the surface. This finding provides a natural explanation for the remarkable inertness of the $CePt_5$ intermetallic. Implications of the structural relaxations determined by LEED-IV analysis are discussed with regard to observations by scanning tunneling microscopy and electron spectroscopies.

DOI: 10.1103/PhysRevB.92.195427 PACS number(s): 68.35.bd, 61.05.J−

I. INTRODUCTION

While primarily interested in genuine electronic properties of rare-earth-element-derived intermetallic phases at surfaces, Tang *et al.* also noticed unusually low sticking coefficients for molecular adsorption in their first report on ordered Ce-Pt surface alloys [1]. Both aspects have since generated continued interest and led to investigations on correlated electron behavior [2–5] and surface chemistry [6–11]. In both fields, knowledge of the surface structure is often of paramount importance for gaining an understanding of observed behaviors. Based on adsorption studies [9–11] it was suggested that the surfaces generated by alloying Ce into Pt(111) should mostly be terminated by Pt atoms alone. Characteristic spatially periodic signatures observed by scanning tunneling microscopy (STM) [8,12] are consistent with the presence of kagome holes in the terminating Pt layer, which are characteristic structural elements of several crystalline bulk Ce-Pt phases [9,13]. Based on an analysis of vibrational frequencies of adsorbed molecules, Essen *et al.* argue, however, that adsorption at such sites does not occur [9]. In a most recent theoretical analysis of (sub-) surface atomic geometries and associated energetics, Tereshchuk *et al.* conclude that the surfaces should indeed be Pt terminated and that the kagome hole sites should be occupied by additional Pt atoms, resulting in a dense Pt surface atomic layer [14]. In a recent piece of work [5] a large body of evidence was presented which supports earlier assumptions [4,8] that the intermetallic phase does possess $CePt_5$ stoichiometry over a wide range of surface alloy thickness. In the present work, we experimentally address the surface termination of this surface intermetallic by energy-dependent low energy electron diffraction (LEED) and corresponding LEED-IV analysis.

II. EXPERIMENTAL PROCEDURE AND LEED-IV SIMULATION

A. Experimental

The preparation of $CePt_5$/Pt(111) specimens is well documented in the literature [1,8,9,12]. Experiments were conducted in an ultrahigh vacuum chamber (base pressure $<2 \times 10^{-10}$ mbar) equipped with the necessary tools for *in situ* surface preparation, Ce deposition, and monitoring, as well as a LEED unit. Specimen temperatures were measured with an infrared pyrometer. Clean Pt(111) surfaces were prepared by repeated cycles of 1 keV Ar^+ ion sputtering and annealing to 1170 K. Cerium (purity 99.9%) was evaporated onto Pt(111) near room temperature from a thoroughly outgassed tungsten crucible with a commercial electron beam evaporator. The sample manipulator was equipped with a quartz microbalance (QMB), mounted in a position adjacent to the sample, allowing us to rapidly switch between exposure of the QMB and the specimen to the Ce evaporate. The Ce deposition rate was monitored and checked for stability with the QMB just before deposition. Subsequently, the Pt crystal was annealed to approximately 970 K for 5 to 10 min. This procedure yields the known, well-ordered, and remarkably inert Ce induced reconstructions [1,8,9,12].

Before proceeding to LEED-IV experimentation, the surfaces were checked for absence of spurious oxide contaminations which are known to produce additional LEED spots [6,9,15]. LEED-IV data sets were generated from images of the diffraction patterns taken at ambient temperature in the kinetic energy range of 35 eV $< E_{\mathrm{kin}} <$ 120 eV in 1-eV increments with a charge-coupled-device camera. The sample was deliberately positioned with a polar misorientation of approximately 1° with respect to normal incidence for recording the diffraction patterns. In this way, nominally equivalent diffraction spots yield systematic differences in their IV curves that should be reproduced in the LEED-IV simulations. A total of 16 first- and second-order diffraction spots (see Fig. 1) was included in the analysis. Spot intensities were extracted semiautomatically from the series of images using custom-developed codes for spot tracking and background subtraction [16]. In preparation for the IV analysis, three-point adjacent averaging was applied to the extracted data and the resulting IV curves were sampled at 3-eV intervals, in correspondence with the energy increments of the LEED-IV simulation and analysis described below.

B. LEED-IV simulations

LEED-IV simulations and optimization were calculated with the CLEED package [17]. Atomic scattering phase shifts

*fauth@physik.uni-wuerzburg.de

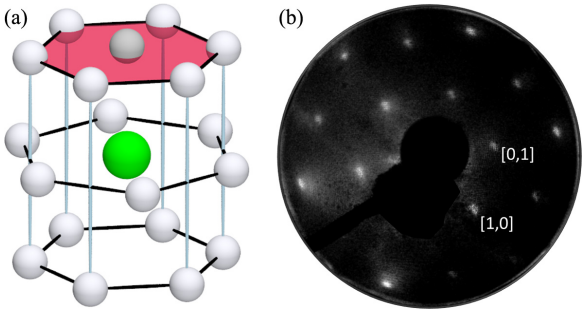

FIG. 1. (Color online) (a) Hexagonal surrounding of a Ce atom (large green sphere) in $CePt_5$. The bottom layer exhibits the kagome hole characteristic of the bulk structure. The top layer includes an extra Pt atom as suggested for the surface layer. Its vertical displacement indicates the possibility of relaxation. (b) LEED image of $CePt_5$/Pt(111) at $t_{nom} = 4$ u.c. taken at $E_{kin} = 60$ eV. Basic LEED beam indexation is indicated. The sample is tilted by approx. 1° with respect to normal electron incidence.

were computed up to angular momentum $l_{max} = 9$ by means of the package by Barbieri and van Hove [18] with the parameters given in Table I.

Xα exchange potential paramaters α were taken from Ref. [19] and weighted according to the $CePt_5$ stoichiometry, since the phase shift package only accepts a single α parameter. Since they are very similar in any case, this procedure is unlikely to produce significant errors. The muffin-tin radius for Ce was chosen on the basis of the bulk $CePt_5$ lattice parameters. Within $CePt_2$ layers, the Pt atoms provide a hexagonal surrounding to the Ce atoms with a Pt-Pt distance of 2.68 Å. Representing the Pt atoms by touching spheres, they inscribe a circle of radius $R_{Ce} = 1.75$ Å which was accordingly chosen as the Ce muffin-tin radius. For the Pt atoms we have taken the value determined by Materer *et al.* in their LEED-IV analysis of Pt(111) [20]. This choice has produced excellent results in our own experiments on Pt(111), yielding full agreement with Ref. [20]. Attempts to compute the Ce phase shifts at the Hartree Fock (HF) level produced erroneous results associated with the $4f^1$ configuration. We resorted to their calculation in the local density approximation (LDA) instead. To check the consequences of this choice, we calculated the phase shifts for Lanthanum at both the HF and LDA levels, respectively, for comparison. Appreciable differences occurred at energies below 30 eV exclusively, outside the experimental energy range of the present study.

Within CLEED the downhill simplex algorithm was used to minimize the Pendry reliability factor R_P [21] under variation of the free parameters of proposed structural models, which we shall discuss in detail below. The near-surface geometry is divided into a "bulk" part with fixed geometry and an "overlayer" part where the atomic positions within the surface unit cell are allowed to relax such as to improve the agreement between calculated and measured IV curves. Multiple scattering between layers ("bulk" and "overlayer") is effectively calculated using layer doubling [22]; scattering within layers with more than one atom per unit cell is treated using the combined space method [23]. Both formalisms treat multiple scattering to infinite order. In addition to the structural overlayer parameters, the polar and azimuthal angles of the incoming electron beam are also treated as free parameters.

The dimensions of "bulk" and "overlayer" unit cells, average thermal atomic root-mean-square displacements, and imaginary part of the optical potential are parameters that require optimization outside the simplex algorithm. A multitude of systematic scans in parameter space were performed in an iterative manner to find the optimum parameters for the structural models considered.

TABLE I. Input parameters to the phase shift calculations. Values for the Xα exchange potential α according to Ref. [19], their stoichiometry weighted average was taken for the actual calculation. Choice of muffin tin radii R_{mt} and computational method are discussed in the text.

Element	Z	Configuration	α	R_{mt} (Å)	Method
Ce	58	$[Xe]4f^15d^16s^2$	0.69845	1.75	LDA
Pt	78	$[Xe]4f^{14}5d^96s^1$	0.69306	0.95	HF

C. Structural models

In accordance with our previous findings concerning structure and composition of the Ce induced reconstructions [5,12], we have taken $CePt_5$ composition and hexagonal symmetry for granted in our approach. This considerably limits the number of structural models to be tested. They all relate to the basic atomic arrangement of $CePt_5$ as depicted in Fig. 1(a). While our main concern is to determine the surface termination, the LEED-IV analysis also enables us to draw some interesting conclusions concerning relaxation of atomic positions near the surface.

As outlined in Refs. [5] and [12], $CePt_5$/Pt(111) usually forms as an ultrathin film of well defined thickness t_{nom}, which may be expressed in terms of the number of $CePt_5$ unit cells (u.c.) it encompasses. At $t_{nom} = 3$ u.c., a corrugated surface forms in which the in-plane $CePt_5$ unit cell dimension amounts to $10/9\sqrt{3}d_{nn}^{Pt} \approx 5.33$ Å, where d_{nn}^{Pt} is the next neighbor distance in the Pt(111) substrate. Registry to the substrate is realized by forming a large $(3\sqrt{3} \times 3\sqrt{3})R30°$ supercell. The superstructure formation causes satellite LEED spots to occur with appreciable intensity [1,8,9]. At $t_{nom} = 4$ u.c., where the present LEED-IV data were taken, the corrugation is markedly reduced and the LEED satellite intensities drop to below detection threshold [12]. In our simulation, we therefore neglect this superstructure formation. Likewise, due to the small probing depth at the small electron energies employed, the substrate diffraction spots have ceased to contribute to the LEED diffractograms at this thickness and its presence is neglected altogether.

We thus represent our specimen exclusively by the $CePt_5$ bulk lattice, reducing the effect of the substrate to a modification of the lattice parameter only. Of the four $CePt_5$ unit cells stacked along the surface normal, two are regarded belonging to the "bulk" part in the simulation, limiting further relaxation to the remaining atomic layers. LEED-IV calculations and optimization were performed for three different surface terminations. Model C is terminated by a $CePt_2$ atomic layer, as represented in Fig. 2(a), and corresponds to the central

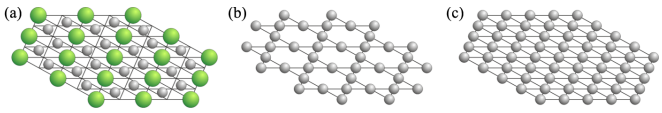

FIG. 2. (Color online) Illustration of the three different termination layers considered. (a) $CePt_2$ layer (model C). (b) Pt kagome layer (model K). (c) Pt layer with filled kagome holes (model P).

atomic layer in Fig. 1(a). This model is the least likely given the inertness of the surface found in the majority of adsorption experiments [8,9,11]. The other two models are terminated by variants of a pure Pt layer, a kagome net [model K, Fig. 2(b)] on the one hand and a configuration in which the kagome holes are filled with additional Pt atoms [model P, Fig. 2(c)] on the other. These configurations may be seen as to be in accordance with existing interpretations of STM topographies [8,12] and theoretical results [14], respectively.

The resulting three models are summarized in Fig. 3, which also illustrates our nomenclature with respect to the parameters that characterize the outcome of the LEED-IV analysis. An initial set of optimization runs was calculated for each model, with common initial parameters as summarized in Table II. The interlayer distances were set to equal values, i.e., $c_{\mathrm{bulk}} = c_1 = \cdots = c_4$ (where applicable), with initial values ranging between 2.05 and 2.30 Å. Thermally induced atomic motion is accounted for through corresponding root-mean-square displacements Δr_{Ce} and Δr_{Pt}.

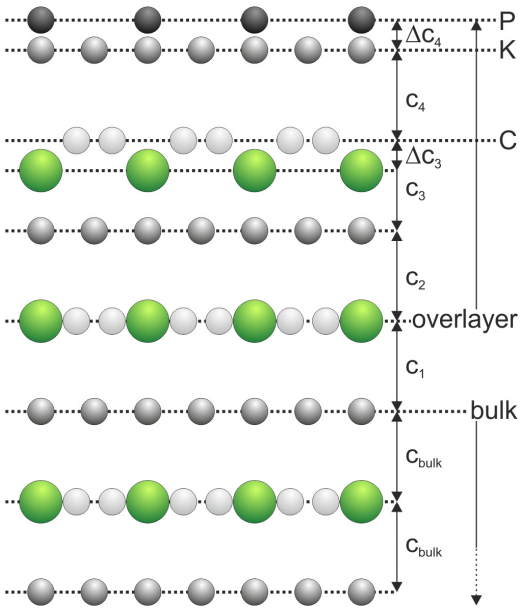

FIG. 3. (Color online) Illustration of the three structural models for $CePt_5$/Pt(111). The two $CePt_2$ layers nearest to the Pt(111) interface are represented by a rigid $CePt_5$ lattice with full bulklike symmetry and equidistant atomic layer spacing c_{bulk}. The following two layers were allowed to independently relax along the surface normal (parameters c_1, c_2). Pt and Ce atoms are allowed to individually relax (parameters c_3, Δc_3) in the final $CePt_2$ layer which terminates model C. Model K assumes the presence of an additional kagome layer at distance c_4, the holes of which are filled by additional Pt atoms at position Δc_4 in model P.

TABLE II. Common initial parameters for first round of LEED-IV calculations.

$V_{o,i}$	$\Delta r_{\mathrm{Ce,Pt}}$	θ_i	φ_i	a	Δc_3, Δc_4[1]
4 eV	0.05 Å	1°	60°	5.33 Å	0

[1]Where applicable.

The best R_{P} factors obtained for the models C, K, and P were $R_{\mathrm{P}}^{\mathrm{C}} = 0.561$, $R_{\mathrm{P}}^{\mathrm{K}} = 0.423$, and $R_{\mathrm{P}}^{\mathrm{P}} = 0.290$, with Pendry double reliability factors [21] around RR = 0.17 in all cases. On this basis, models C and K could both have been eliminated from further consideration. Nevertheless, we have carried out the full LEED-IV optimization for both models K and P, respectively.

III. RESULTS AND DISCUSSION

Upon completing the full set of optimization runs, the Pendry factors were considerably improved, while the preference for model P remained. The resulting parameters characterizing the $CePt_5$/Pt(111) system at $t_{\mathrm{nom}} = 4$ u.c. are summarized in Table III.

The LEED-IV analysis thus confirms the conclusion drawn from adsorption studies [9,10] concerning Pt termination of $CePt_5$/Pt(111). It is also fully in line with the recent suggestion on theoretical grounds that the surface layer contains no kagome holes, their sites actually being filled with additional Pt atoms [14]. This finding offers a most natural explanation for the remarkable inertness of these surfaces.

There are a number of further noteworthy observations to be made on the basis of the optimized parameters. Judging by the respective R factors, model P is clearly to be preferred. We notice that the polar specimen tilt angle is well accounted for in this case (Table III and Fig. 4 in the appendix), while the fitting procedure "sacrifices" agreement in θ_i for better overall reduction of R_{P} in case of model K. As a consequence, the intensity variations generated by the tilt angle are poorly reproduced in the calculated LEED-IV curves for model K (see the Supplemental Material Ref. [24]).

The overall $R_{\mathrm{P}} = 0.259$ after complete optimization is relatively large compared to considerably smaller values reported in the literature for noble and transition metal systems and surface alloys [20,25–27]. This, however, appears to be a general trend for systems containing rare-earth elements; R_{P} values comparable to or larger than ours have consistently been obtained in such cases [28–31]. This finding may hint at difficulties to correctly describe rare-earth atoms within the current status of the dynamical scattering formalism, but it could also derive from inhomogenieties in the intermetallic layer thickness and some surface roughness which have led to increased R factor values in the past [32,33].

The in-plane lattice parameter a at $t_{\mathrm{nom}} = 4$ u.c. is found to be increased with respect to its value [12] at $t_{\mathrm{nom}} = 3$ u.c. This can be understood as a relaxation towards the intrinsic bulk lattice parameter of $CePt_5$. Interestingly, since the registry to the underlying Pt(111) lattice is unchanged [12], this finding signifies that a considerable portion of the interfacial stress is accommodated as tensile strain in the Pt substrate. A similar observation, yet with opposite sign, holds for the terminating

TABLE III. Final R factors, optimized nonstructural and optimum structural parameters (all lengths given in Å) for models P and K, respectively, after the full LEED-IV optimization runs. Error estimates determined by Pendry's RR method [21] are given in parentheses.

Model	R_P	RR	θ_i (°)	φ_i (°)	$V_{o,i}$ (eV)	Δr_{Ce}	Δr_{Pt}	a	c_{bulk}	c_1	c_2	c_3	Δc_3	c_4	Δc_4
P	0.259	0.131	1.22(12)	66.5(5)	2.4	0.05	0.07	5.35	2.07	2.33(18)	2.13(31)	2.30(24)	0.23(17)	2.28(17)	0.22(14)
K	0.351	0.131	0.38(14)	66(3)	2.4	0.04	0.02	5.35	2.16	2.36(12)	1.78(27)	2.72(21)	0.18(15)	1.91(14)	—

Pt layer: With the kagome holes filled, this layer is actually compressed when compared to the Pt(111) surface.

The positive value of Δc_4 indicates that this stress is relieved through a protrusion of the Pt atoms in the kagome hole positions with respect to the surrounding atoms by about 0.2Å. The subsurface Ce atoms are displaced downwards with respect to their in-plane neighbors by a similar distance. A small protrusion, although not quantified, is also indicated in the theoretical results of Tereshchuk *et al.* [14]. Such a protrusion, however, has never been observed by STM. The constant current topographies as well as differential conductance maps in Refs. [8] and [12] rather feature local depressions with unit cell periodicity instead, while absence of such corrugation (using different tunneling parameters) was reported in Ref. [10]. Our findings indicate that these observations are likely to be caused by the electronic structure rather than the surface geometry and may relate to local charge transfer from the neighboring Lanthanide atom in the subsurface layer.

Finally, the need to assume a reduced lattice parameter c_{bulk} along the surface normal in the "bulk" part of the specimen comes as a surprise, given the fact that the lattice is also laterally compressed compared to bulk $CePt_5$. This behavior, while reminiscent of auxetic materials, is most likely also related to electronic interactions at the interface to the substrate. Indeed, electron spectroscopies reveal an increased hybridization between the localized Ce $4f$ and itinerant electrons in the thickness range of just a few unit cells [1,5]. While the associated change in Ce valence is less pronounced than, e.g., in the isostructural γ- to α-Ce transition [34], the qualitative and spectroscopic behavior [35] appears related. Further work aimed at shedding more light on these interesting interfacial properties is currently underway.

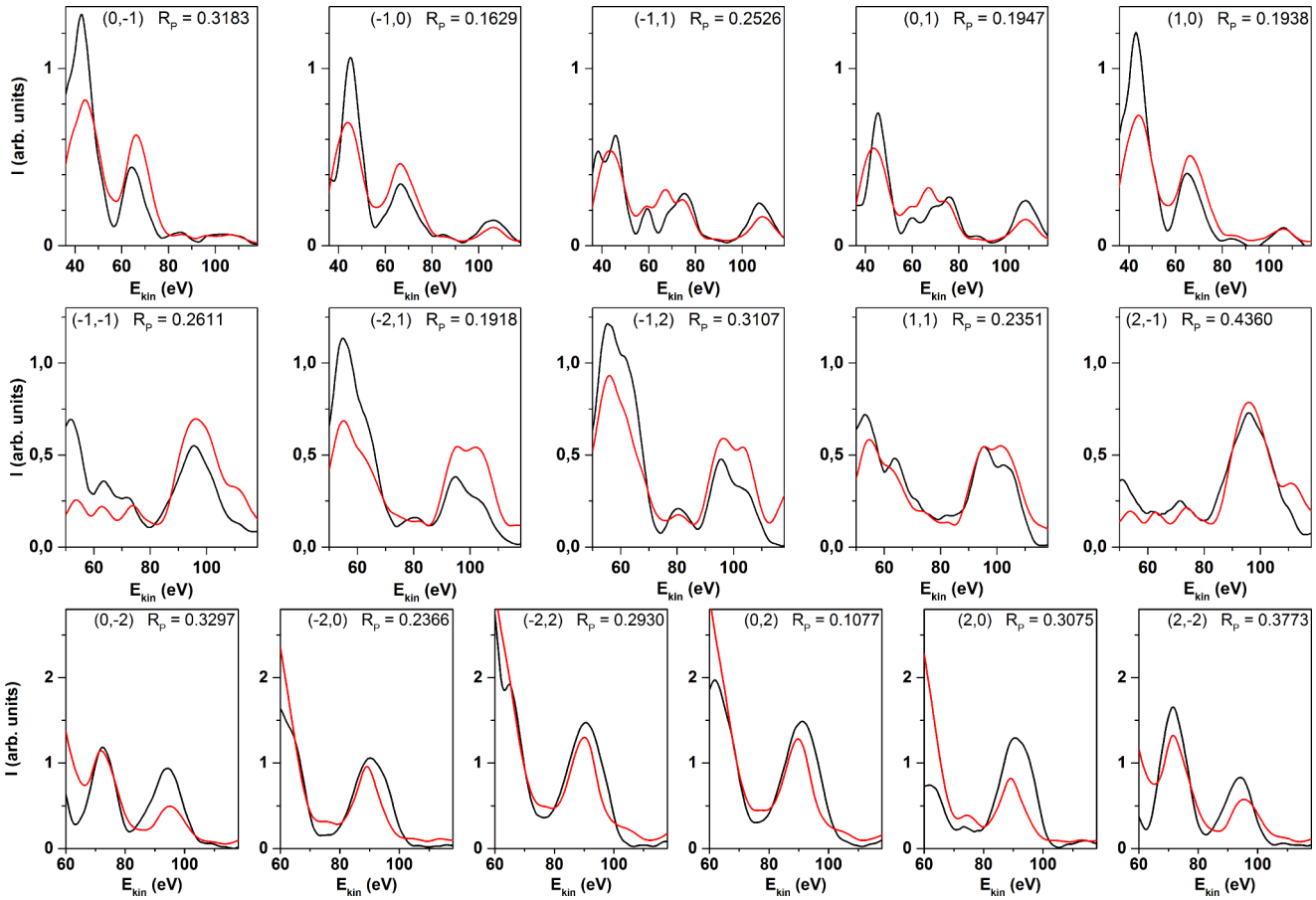

FIG. 4. (Color online) Full LEED-IV results for model P. Intensities of calculated curves (in red) have been scaled such as to yield the same integrated intensities as the experimental ones (in black).

IV. CONCLUSIONS

We have presented a LEED-IV study of the surface termination of the $CePt_5$/Pt(111) system. Our findings demonstrate that the remarkable inertness of these surfaces derives from pure Pt termination, where the kagome holes, which are present in the hexagonal bulk $CePt_5$ lattice, are filled with additional Pt atoms at the surface. This observation is well in line with recent theoretical predictions. Indirectly, our study provides interesting hints at electronic properties related to the surface of the intermetallic compound, as well as its interaction with the Pt(111) substrate. In particular, the $CePt_5$ lattice appears to be considerably contracted near the interface, in line with the observation of increased hybridization of Ce $4f$ and itinerant electrons at or near the interface.

ACKNOWLEDGMENT

The Würzburg authors (C.P., M.Z., and K.F.) gratefully acknowledge the financial support by the Deutsche Forschungsgemeinschaft within FOR1162 (TP 7).

APPENDIX: FULL LEED-IV DATA SET FOR MODEL P

Figure 4 displays the full set of measured and calculated LEED-IV curves for model P. A corresponding figure for model K is provided in the Supplemental Material.

[1] J. Tang, J. M. Lawrence, and J. C. Hemminger, Phys. Rev. B **48**, 15342 (1993).
[2] A. B. Andrews, J. J. Joyce, A. J. Arko, J. D. Thompson, J. Tang, J. M. Lawrence, and J. C. Hemminger, Phys. Rev. B **51**, 3277 (1995).
[3] M. Garnier, D. Purdie, K. Breuer, M. Hengsberger, and Y. Baer, Phys. Rev. B **56**, R11399(R) (1997).
[4] M. Klein, A. Nuber, H. Schwab, C. Albers, N. Tobita, M. Higashiguchi, J. Jiang, S. Fukuda, K. Tanaka, K. Shimada, M. Mulazzi, F. F. Assaad, and F. Reinert, Phys. Rev. Lett. **106**, 186407 (2011).
[5] C. Praetorius, M. Zinner, A. Köhl, H. Kießling, S. Brück, B. Muenzing, M. Kamp, T. Kachel, F. Choueikani, P. Ohresser, F. Wilhelm, A. Rogalev, and K. Fauth, Phys. Rev. B **92**, 045116 (2015).
[6] P. Luches, F. Pagliuca, and S. Valeri, J. Phys. Chem. C **115**, 10718 (2011).
[7] P. Malacrida, M. Escudero-Escribano, A. Verdaguer-Casadevall, I. E. L. Stephens, and I. Chorkendorff, J. Mater. Chem. A **2**, 4234 (2014).
[8] C. J. Baddeley, A. W. Stephenson, C. Hardacre, M. Tikhov, and R. M. Lambert, Phys. Rev. B **56**, 12589 (1997).
[9] J. M. Essen, C. Becker, and K. Wandelt, e-J. Surf. Sci. Nanotech. **7**, 421 (2009).
[10] U. Berner and K. D. Schierbaum, Phys. Rev. B **65**, 235404 (2002).
[11] B. Vermang, M. Juel, and S. Raaen, Phys. Rev. B **73**, 033407 (2006).
[12] J. Kemmer, C. Praetorius, A. Krönlein, P.-J. Hsu, K. Fauth, and M. Bode, Phys. Rev. B **90**, 195401 (2014).
[13] A. Janghorban, M. Lomello-Tafin, J. M. Moreau, and P. Galez, Intermetallics **18**, 2208 (2010).
[14] P. Tereshchuk, M. J. Piotrowski, and J. L. F. Da Silva, RCS Adv. **5**, 521 (2015).
[15] K. D. Schierbaum, Surf. Sci. **399**, 29 (1998).
[16] P. Sprau, R. Fradczyk, and K. Fauth (unpublished).
[17] Manual available from the authors.
[18] A. Barbieri and M. van Hove (private communication); contact G.H. (g.held@reading.ac.uk).
[19] K. Schwarz, Theor. Chim. Acta **34**, 225 (1974).
[20] N. Materer, U. Starke, A. Barbieri, R. Döll, K. Heinz, M. A. van Hove, and G. Somorjai, Surf. Sci. **325**, 207 (1995).
[21] J. B. Pendry, J. Phys. C **13**, 937 (1980).
[22] J. B. Pendry, *Low Energy Electron Diffraction* (Academic Press, London, 1974).
[23] M. A. V. Hove and S. Y. Tong, *Surface Crystallography by LEED*, Springer Series in Solid State Sciences (Springer, Berlin, 1979).
[24] See Supplemental Material at http://link.aps.org/supplemental/10.1103/PhysRevB.92.195427 for a pdf containing the full set of atomic positions and a data file of the LEED IV dataset used as input for the simulations.
[25] S. Walter, H. Baier, M. Weinelt, K. Heinz, and T. Fauster, Phys. Rev. B **63**, 155407 (2001).
[26] S. Gallego, C. Ocal, M. C. Munoz, and F. Soria, Phys. Rev. B **56**, 12139 (1997).
[27] H. A. Etman, Z. V. Zheleva, G. Held, and R. A. Bennett, J. Phys. Chem. C **115**, 4191 (2011).
[28] J. Quinn, Y. S. Li, F. Jona, and D. Fort, Surf. Sci. **257**, L647 (1991).
[29] J. Quinn, Y. S. Li, F. Jona, and D. Fort, Phys. Rev. B **46**, 9694 (1992).
[30] J. Giergiel, A. W. Pang, H. Hopster, X. Guo, S. Y. Tong, and D. Weller, Phys. Rev. B **51**, 10201 (1995).
[31] C. Bonet, D. J. Spence, and S. P. Tear, Surf. Sci. **504**, 183 (2002).
[32] S. R. Puisto, G. Held, V. Ranea, S. J. Jenkins, E. E. Mola, and D. A. King, J. Phys. Chem. B **109**, 22456 (2005).
[33] G. Jones, M. J. Gladys, J. Ottal, S. J. Jenkins, and G. Held, Phys. Rev. B **79**, 165420 (2009).
[34] D. C. Koskenmaki and K. A. Gschneidner, Jr., in *Handbook on the Physics and Chemistry of Rare Earths* (Elsevier, Amsterdam, 1978), Vol. 1, chap. 4, p. 337.
[35] C. Dallera, M. Grioni, A. Palenzona, M. Taguchi, E. Annese, G. Ghiringhelli, A. Tagliaferri, N. B. Brookes, T. Neisius, and L. Braicovich, Phys. Rev. B **70**, 085112 (2004).